**Paper # A05** **Topic: Laminar Flames**

5th US Combustion Meeting
Organized by the Western States Section of the Combustion Institute
and Hosted by the University of California at San Diego
March 25-28, 2007.

# Effect of NO on extinction and re-ignition of vortex-perturbed hydrogen flames

*Uen Do Lee, Sebastian A. Kaiser, Chun Sang Yoo, Jacqueline H. Chen, and Jonathan H. Frank*

*Combustion Research Facility, Sandia National Laboratories*
*7011 East Ave, Livermore, CA 94551-0969, USA*

The catalytic effect of nitric oxide (NO) on the extinction and re-ignition of a vortex-perturbed hydrogen/air diffusion flame is studied in a heated counter-flow configuration. Nitrogen-diluted hydrogen at room temperature is burned with air heated to approximately the auto-ignition temperature. Localized extinction is induced by a fuel-side toroidal vortex, and the recovery process of the extinguished region is monitored by planar laser-induced fluorescence of the hydroxyl radical (OH). The addition of a small amount of NO significantly alters the re-ignition process by shifting the balance between chain-termination and chain-branching reactions. Without NO doping, the flame recovery process is mainly governed by edge-flame propagation. With NO doping, however, auto-ignition occurs in the center of the extinguished region, and the flame recovers by a merging between the central re-ignition kernel and the annular edge-flame. The influence of NO on the re-ignition is investigated as a function of fuel concentration and air temperature. Experimental results are compared to direct numerical simulations. This combined experimental and numerical study provides detailed insight into the interaction between transient flows and ignition processes.

## 1. Introduction

Flame extinction and re-ignition are important processes that determine the operating envelope of practical combustors, and an improved understanding of the coupling between ignition chemistry and transient flows is needed. Accurate modeling of extinction and re-ignition in turbulent flames remains a challenge especially for the stabilization and partial quenching structure of turbulent flames [1]. Recently, PDF models have shown promise for modeling turbulent jet flames [2]. If the extinction and re-ignition can be controlled by a small amount of additive, it will have a great impact on the design and operation of practical combustion systems. Reciprocating engines with exhaust-gas recirculation, flame stabilization with back-mixing of product gases in gas turbine combustors, high temperature combustion of syngas or heat regenerating systems are of particular interest [3,4]. The interactions between $NO_x$ (NO and $NO_2$) and the oxidation of fuel has been referred to as "mutual sensitization", and catalytic effects of NO on the oxidation of fuels as well as the promoting action of hydrocarbons on the conversion of NO to $NO_2$ are representative effects [5-19]. The catalytic effect of NO on extinction and re-ignition can lead to change in the auto-ignition timing of reciprocating engines (i.e. engine knock and modified onset of low temperature combustion in HCCI engines), and more fundamentally, to change in system properties such as flammability limit and flame stabilization conditions. On the other hand, the conversion of NO to $NO_2$ is important for the

modeling of the $NO_x$ emission from combustion systems and for the development of $DeNO_x$ technologies [5]. Recently, the accelerating and inhibiting characteristics of NO on the oxidation of n-heptane, iso-octane, toluene [6], methanol [6,8,9], n-butane [7], ethane [10], Dimethyl ether (DME) [11], methane [12], propane [13], and 1-pentene [14] have been reported. In diesel combustion, the influence of NO on the combustion phasing in an HCCI engine has been studied [19], and nitrate additives, such as 2-ethylhexyl nitrate (2-EHN), can be used to provide a source of $NO_2$ for reducing ignition delay times [20]. For hydrogen, the impact of NO on kinetics has been well established as a catalyst which significantly alters the balance between the chain terminating steps related to $HO_2$ formation ($H + O_2 + M \Leftrightarrow HO_2 + M$) and chain-branching steps related to OH formation ($NO + HO_2 \Leftrightarrow NO_2 + OH$, $NO_2 + H \Leftrightarrow NO + OH$) [15-19,32,42,43]. Regarding the catalytic effect of NO, most previous studies were conducted in a homogeneous environment [5-17] and a steady configuration [18]. However, it is also necessary to investigate the coupling between transient transport and ignition chemistry, including the catalytic effect of NO, because nearly all practical applications of combustion involve a nonpremixed, highly convective-diffusive environment including interactions with unsteady flow. For such fundamental investigations, a highly repeatable experiment with well-controlled boundary conditions is desirable. Moreover, a relatively simple flow configuration allows for the benefits of detailed numerical simulations with reasonable computational expense. Therefore, in the present study we investigate the effect of NO on extinction and re-ignition using a vortex-perturbed flame, with addition of NO to the hot oxidizer stream.

The flame-vortex interaction configuration has been extensively used to understand the transient response of the inner structure of non-premixed flames [21-23], ignition in unsteady flow [24,26], and dynamics of edge-flame propagation [27-31]. In the present experiment, localized extinction is induced by a fuel-side vortex and the recovery process of the extinguished region is monitored with OH PLIF. A re-ignition kernel forms in the extinguished region when the air flow is heated to a temperature above the ignition limit. The influence of NO on this ignition process is investigated as a function of fuel concentration and air temperature with a constant vortex strength and initial strain rate. The interactions between transient flow, the central re-ignition kernel, and boundary edge-flames generate very interesting phenomena. Various modes of recovery of the extinguished region have been observed. Addition of a small amount of NO in the hot air stream significantly alters the re-ignition process and drastically changes the recovery mechanisms. To understand the catalytic effect of NO-addition on extinction and re-ignition, direct numerical simulations (DNS) are conducted in the same general configuration as the experiment. The simulations employ detailed chemistry incorporating recent NO reaction mechanism [32]. The coupling between experiment and simulation allows for investigation of a broad parameter space and identification of the key elementary reactions and flow characteristics involved.

## 2. Experimental and numerical methods

### *2.1 Experimental method*

Experiments were performed in laminar opposing flows of heated air and $N_2$-diluted $H_2$ at 298 K using the axisymmetric counter-flow burner shown in Fig. 1. The burner is based on the design described in [24,25] with modifications to provide higher temperatures of heated air and a pulsed vortex generator. The opposing nozzles have an inner diameter of 23 mm and are separated by a

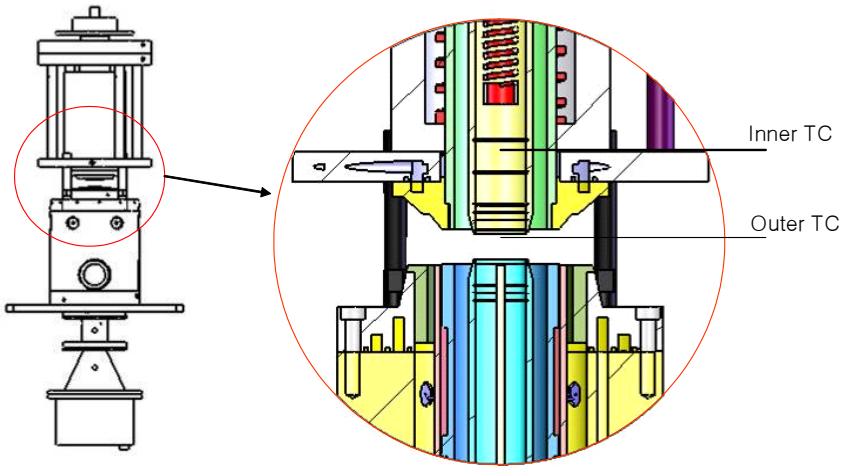


**Figure 1: Counter-flow jets with an air-heating system**

distance of 12 mm. The top of the burner is comprised of concentric ceramic tubes with heated air flowing from the central tube. An annular $N_2$ coflow shields the flame from external disturbances. Independently controlled internal (SiC) and external (iron-chrome-aluminum wire ribbon partially embedded in the ceramic fiber) heating elements are capable of heating the air and $N_2$ flows up to a temperature of 1600 K. The air temperature is measured by the inner shielded thermocouple (K-type), and the temperature at the nozzle exit is measured with the outer thermocouple (R-type). Both thermocouples have a wire diameter of 75 μm. The measured temperatures were corrected for radiative heat losses. These corrections account for the view factor of the heated nozzles and mesh, and assumed a constant Nusselt number of 1.6 [33]. At a distance of 1 mm from the top nozzle, the radial temperature variation is less than 5 K over a radius of 5 mm around the center line. Several screens are inserted in the nozzle to straighten the flow field and provide a symmetric temperature distribution. In the bottom burner, a mini nozzle with a diameter of 2 mm was installed to produce a toroidal vortex that is strong enough to locally extinguish the flame on the burner centerline. A loudspeaker with a diameter of 100 mm is mounted onto the large opening of a converging nozzle connected to the mini nozzle. The speaker is surrounded by a sealed housing that is attached to the converging nozzle to eliminate the possibility of gas leakage through the speaker. The loudspeaker is driven by a smoothed saw-tooth waveform with a rapid increase in voltage and a gradual decrease back to the original value. The $H_2/N_2$ mixture that flows through the mini nozzle is identical to that of the main nozzle. The flow rates of gases are measured by mass flow controllers to be within ±1 % for full range and each main reactant stream is surrounded by a nitrogen curtain flow.

The extinction and re-ignition of the flame is recorded by measuring OH planar laser-induced fluorescence (LIF). To excite OH LIF, the frequency-doubled output from a Nd:YAG pumped dye laser is tuned to 282.75 nm to pump the $Q_1 5$ line of the $A^2\Sigma^+ \leftarrow X^2\Pi^+$ ($v' = 1$, $v'' = 0$). The laser beam is formed into a vertical sheet using a 400 mm cylindrical lens. The OH fluorescence is imaged onto an intensified CCD camera (512 × 512, Pixel Vision) with an *f/1.8* Cerco quartz camera lens. Color glass filters (UG-11 and WG-305) are used to block elastic scattering of the laser and transmit the OH fluorescence. The OH LIF measurements are performed in the linear LIF regime using a laser energy of 0.6 mJ/pulse. The OH LIF images are corrected for spatial variation in the laser sheet using acetone LIF to measure the average beam profile.

Prior to each measurement of an extinction/ignition event, a flat counterflow flame is stabilized on the burner. Subsequently, the speaker is pulsed to launch the vortex ring from the fuel side to impinge on the flame. Different phases of the ignition/extinction events are measured by varying the delay time between the speaker pulse and the laser pulse with a digital delay generator. The extinction/ignition events are highly repeatable, and different phases of the temporal evolution are measured in separate events. The repeatability also enables phase averaging of 10 ignition events to improve the signal-to-noise ratio.

### *2.2 Numerical method*

Simulations of a vortex-perturbed hydrogen/air diffusion flame in axisymmetric counterflow are performed to numerically investigate the catalytic effect of NO on extinction and re-ignition. The simulations are performed using the direct simulation code, S3D, which solves the compressible Navier-Stokes, species continuity, and total energy equations. A fourth-order explicit Runge-Kutta method for time integration and an eighth-order central spatial differencing scheme were used [34,35] with a tenth-order filter to remove spurious high-wave number oscillations. A detailed $H_2/O_2/NO_x$ kinetic mechanism [32] was used and CHEMKIN software libraries [36] were linked with S3D to evaluate reaction rates, thermodynamic and mixture-averaged transport properties. The OH mole fraction, $X_{OH,}$ and streamlines from a steady counterflow flame used as the initial condition for the vortex/flame interaction simulations is shown in Fig. 2. The domain size is $L_x \times R$ = 12 mm × 12 mm with 400 grid points in each direction. At the inlet boundaries, the temperature and species mole fractions are specified as $T_1$ = 298 K, $X_{H2,1}$ = 0.125, $X_{N2,1}$ = 0.875, and $T_2$ = 951 K, $X_{O2,2}$ = 0.21, $X_{N2,2}$ = 0.79, where subscripts 1 and 2 denote the fuel and oxidizer streams, respectively. The inlet flows are assumed to be plug flow and the axial velocities are specified as $\overline{V_1}$ = 0.635 m/s and $\overline{V_2}$ = 1.05 m/s such that the overall strain rate based on the oxidizer stream is given by $a$ = 350s$^{-1}$ [37]. Improved nonreflecting inflow/outflow boundary conditions for reacting counterflow simulations [31,38,39] were implemented in S3D. Symmetry conditions were specified at the polar axis. To emulate an impulsively driven axisymmetric vortex into the steady flame from the fuel stream boundary the following velocity profile and time history is prescribed [40]:

$$V_1(r,t) = \overline{V_1} + \frac{1}{2}(U_0 - \overline{V_1}) \cdot \left(1 - \tanh\left(10\,(r / r_0 - 1)\right)\right), \tag{1}$$

where $r_0$ is the radius of the vortex taken to be 1.0mm. $U_0$ is the temporal velocity variation of the vortex at the centerline given by:

$$U_0(t) = \begin{cases} \overline{V_1} + \frac{1}{2}(V_{\max} - \overline{V_1}) \cdot \left(1 + \tanh\left(\frac{(t - t_a)}{\sigma}\right)\right), & t \le t_a + \frac{t_b}{2} \\ \overline{V_1} + \frac{1}{2}(V_{\max} - \overline{V_1}) \cdot \left(1 - \tanh\left(\frac{(t - t_a - t_b)}{\sigma}\right)\right), & t > t_a + \frac{t_b}{2} \end{cases} \tag{2}$$

where $V_{max}$ = 2.0 m/s, $t_a$ = 6 ms, $t_b$ = 12 ms, and $\sigma$ = 2 ms.

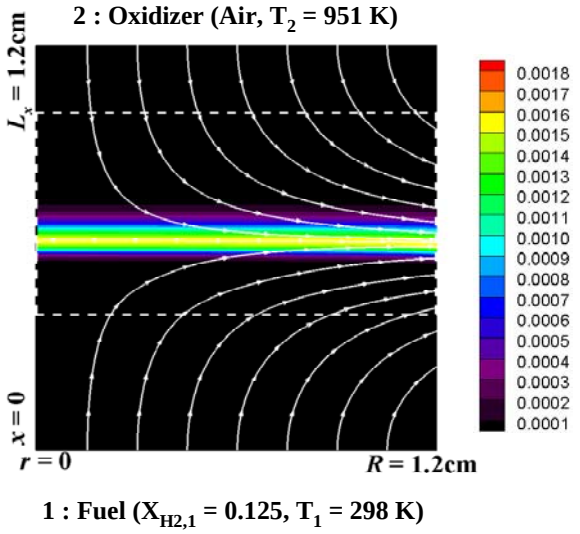


**Figure 2: Isocontours of OH mole fraction in the steady axisymmetric counterflow flame that is used for the initial condition of the numerical simulations. Arrowed lines represent the streamlines of the flow and the dashed line indicates the window for analysis shown in Fig. 8.**

The prescription of the velocity impulse shape and radial velocity variations at the fuel and oxidizer boundaries determines the spatial and temporal variation of the instantaneous scalar dissipation rate as the vortex interacts with the flame. Scalar dissipation rate is an important parameter for extinction and re-ignition. Current efforts to better characterize the velocity impulse and steady velocity profiles at the ambient and heated boundaries should lead to better comparisons between experiment and computation in the future, especially regarding the radial location of extinction and incipient re-ignition.

## 3. Experimental results

The extinction and re-ignition processes are investigated with and without NO doping for a range of air temperatures and fuel concentrations. The different modes of re-ignition are mapped out in a regime diagram for air temperatures above and below the steady-flow auto-ignition temperature. The effects of NO on this regime diagram are explored by repeating the extinction/ignition experiments with NO doped into the heated air flow.

### *3.1 Extinction and re-ignition without NO doping*

We first consider the vortex-flame interaction without NO doping for air temperatures at or below the auto-ignition temperature of the $H_2/N_2$ fuel mixture in a steady counterflow with a global strain rate of a = 350 $s^{-1}$. In this experiment, a steady counterflow flame is established with an air temperature of 951 K, which is slightly above the steady-state auto-ignition temperature. The sequence of OH PLIF measurements in Fig. 3 shows the temporal evolution of the flame as it is perturbed by a fuel-side vortex ring. At 20 ms into the interaction, the vortex ring produces an indent in the flame and induces a thinning of the reaction zone and a reduction of OH near the centerline. Subsequently, this thinned region extinguishes and an annular edge-

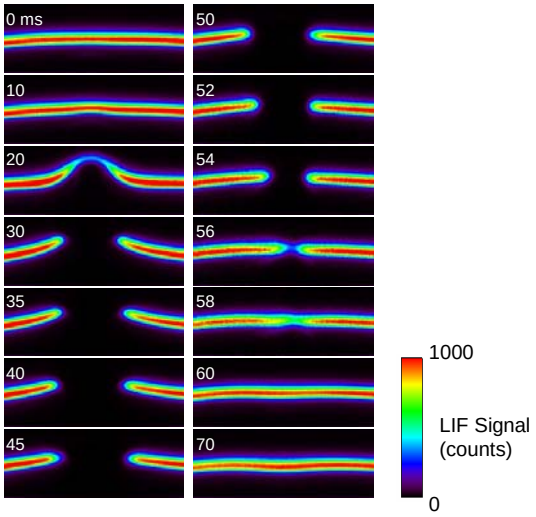


**Figure 3: Sequence of OH LIF images shows the extinction and re-ignition of a counterflow flame during an interaction with a pulsed vortex ring impinging from the fuel side (bottom). The fuel mixture is $X_{H2} = 0.13$, $X_{N2} = 0.87$, and the air is heated to 951 K.**

flame is established. The diameter of the extinguished region remains approximately constant for the time interval from 30 ms to 50 ms. During the 52-56 ms period, the flame recovers as the edge-flame propagates inward toward the centerline. The steady flat flame is re-established at approximately 60 ms into the interaction.

The extinction/re-ignition sequence in Fig. 3 is representative of the flame response for air temperatures from 298 K to slightly above the auto-ignition temperature. For this temperature range and vortex strength, the extinction and re-ignition only occurs when the $H_2$ concentration in the fuel stream is between approximately 12.5 % and 14 %, which is a relatively narrow range. At lower $H_2$ concentrations, it is not possible to stabilize a steady flame, and at larger concentrations the vortex is not strong enough to extinguish the flame. This edge-flame recovery process has been investigated in previous studies [27-31]. A detailed experimental and numerical study of the extinction and re-ignition behavior of counterflow flames with low-temperature reactants is described by Amantini et al. [28,29].

The extinction and re-ignition properties of the vortex-flame interaction change significantly when the air flow is heated above the auto-ignition temperature. At these temperatures, the flame can be stabilized over a broader range of fuel concentrations, and four different modes of flame recovery are observed. The different recovery modes result from a competition between edge-flame propagation and the expansion of an ignition kernel that forms within the extinguished region. For a fixed vortex strength and initial strain rate, these modes are governed by the air temperature and $H_2$ concentration in the fuel stream. Figure 4 shows the regimes of each recovery mode as a function of air temperature and fuel concentration with a constant vortex strength and initial strain rate ($a = 350\ s^{-1}$). The flame response for each regime is illustrated by a sequence of OH LIF images. There are upper limits of fuel concentration where no extinction occurs and lower limits where no flame can be stabilized. The steady ignition limit (triangle symbols) indicates the auto-ignition temperature for different $H_2$ concentrations in a steady counterflow. The recovery by edge-flame propagation is designated as Regime I and is

displayed in Fig. 4g. Note that Regime I extends approximately 10 K above the auto-ignition temperature boundary. For temperatures above the auto-ignition limit, three new recovery modes are observed Mode II, III and IV. A schematic line drawing of all four of the recovery modes is shown below the regime diagram in Fig. 4. For Mode II (Fig. 4a), the annular edge-flame retreats from the centerline until the flame is completely extinguished. Re-ignition occurs by the formation of an ignition kernel near the burner centerline. In this mode, the elapsed time for full recovery is significantly longer than for the other modes since re-ignition is initiated by the relaxation of strain rate after the vortex dissipates. Note that the temperature at the lower boundary of Regime II is below the steady ignition temperature because the strain-rate relaxation in flow trailing the vortex enables the $H_2$/air mixture to ignite at a lower temperature. In Modes III and IV, the flame recovery is a combination of ignition Modes I and II. For Mode III (Fig. 4c), an ignition kernel forms in the center while the edge-flame is retreating. The re-ignition kernel expands to ignite the extinguished region, but the retreating edge-flame extinguishes

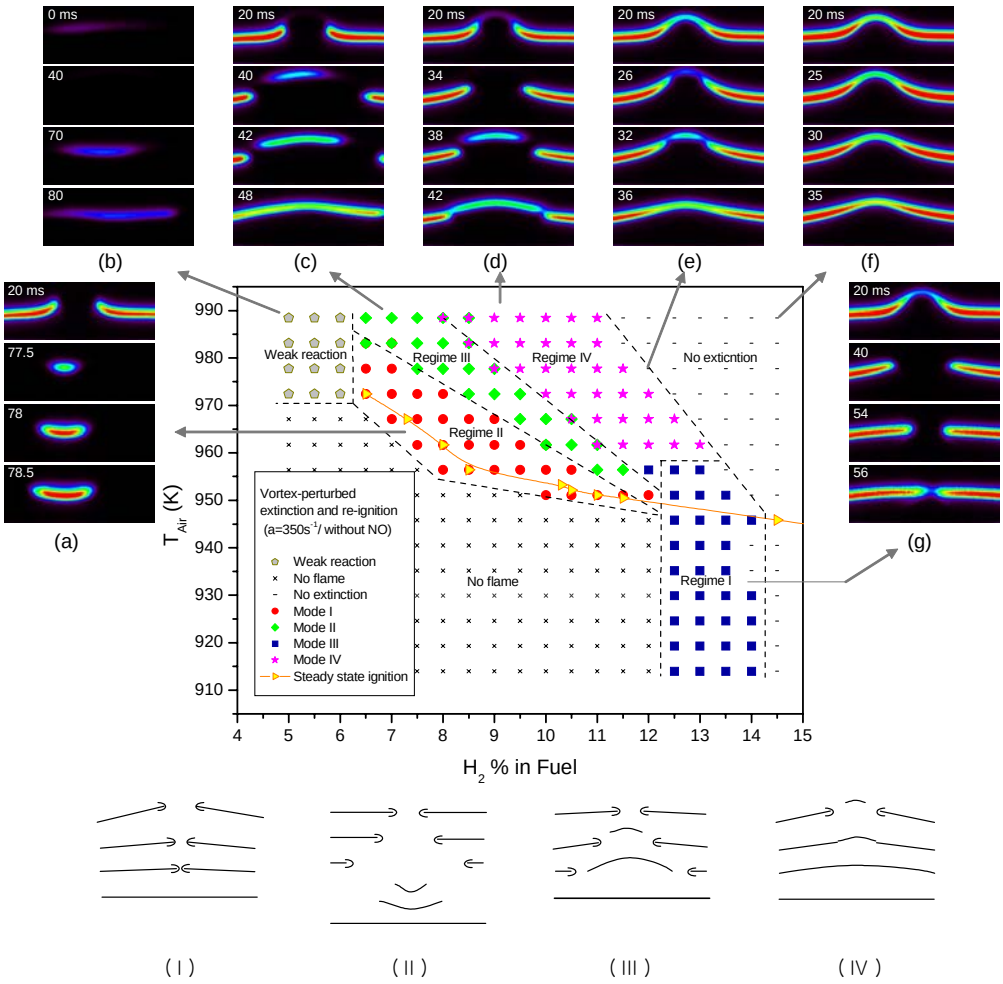


**Figure 4: Regime diagram of recovery process during flame/vortex interaction (a) $X_{H2}$ = 0.11, $T_{air}$ = 951 K (b) $X_{H2}$ = 0.055, $T_{air}$ = 972K (c) $X_{H2}$ = 0.095, $T_{air}$ = 972 K (d) $X_{H2}$ = 0.11, $T_{air}$ = 972 K, $T_{air}$ = 951 K (e) $X_{H2}$ = 0.16, $T_{air}$ = 951 K (f) $X_{H2}$ = 0.13, $T_{air}$ = 951 K. Schematic line diagrams below the regime diagram illustrate the flame recovery process in the four regimes.**

before the ignition kernel can merge with it. We can expect some interactions between the edge-flame and re-ignition kernel. For example, the gas expansion from the kernel increases the flow velocity and enhances the retreating of the edge-flame. Mode IV (Fig. 4d) is characterized by a merging of the central re-ignition kernel and the annular edge-flame. In this mode, the annular edge-flame remains strong and merges with the central ignition kernel. This combination of ignition processes significantly decreases the time for complete recovery of the flame. To understand the limits of these ignition/extinction regimes, it is instructive to consider the flame behavior at the regime boundaries. For example, Fig 4b shows that Regimes II and III are bounded by conditions with 'Weak reaction' when the fuel concentration is low and the air temperature is high. For these conditions, the intensity of the OH LIF signal is very low, and the reaction zone is unstable. Fig. 4e shows the 'No extinction' case that is observed in the upper boundary of Regimes I and IV. In this case, the intensity of the OH LIF signal becomes very low in the vicinity of the vortex, indicating that OH production rates are significantly reduced and the flame is on the verge of extinction. If the fuel concentration is increased further, the flame becomes stronger, and there is no extinction at all, as shown in Fig. 4f.

The 'No flame' region in Fig. 4 indicates the conditions for which a steady counterflow flame cannot be stabilized. Regime I is bounded by the 'no flame' region at a $H_2$ concentration of 12.5 %. A transition from the 'no flame' region to Regimes II, III, and IV occurs with increasing air temperature. The increased temperature enables the formation of the centerline ignition kernel that plays a key role in Regimes II, III, and IV. In contrast, a transition to Regime I is not possible without an increase in fuel concentration. This result indicates that edge-flame propagation, which is the sole ignition mechanism for Regime I, is relatively insensitive to temperature increases. For temperatures above 960 K, Regime I is not accessible. Therefore, re-ignition by the formation of ignition kernels is the dominant mechanism that controls flame recovery at high temperatures.

### *3.2 Catalytic effect of NO on extinction and re-ignition*

The effect of NO on the flame recovery process is investigated by doping the heated air flow with 160 ppm of NO and repeating the vortex-flame experiments over a wide range of air temperatures and $H_2$ concentrations. The NO doping is accomplished by replacing the $N_2$ in air with a mixture of NO in $N_2$.

Figure 5 shows the effect of NO on the flame recovery process at three different conditions. For each condition, the left series of images shows the flame recovery without NO, and the right series shows the re-ignition with NO doping. Remarkably, a small amount of NO enhances the recovery process and causes transfer of the ignition regime. In Figs. 5a and 5c, the recovery process without NO is governed by edge-flame propagation. With NO doping, however, auto-ignition occurs in the center, and the flame recovers by a merging of the central re-ignition kernel and the outer edge-flame. This transformation of the recovery mechanism reduces the recovery time up to 5 ms and 15 ms for the cases of Figs. 5a and 5c, respectively. Fig. 5b shows the transition from Mode II to Mode IV due to the addition of NO. Without NO doping, the flame recovers by re-ignition after complete extinction (Mode II). With NO doping, however, the flame recovers as Mode IV and the reduction of the full recovery time is about 25 ms.

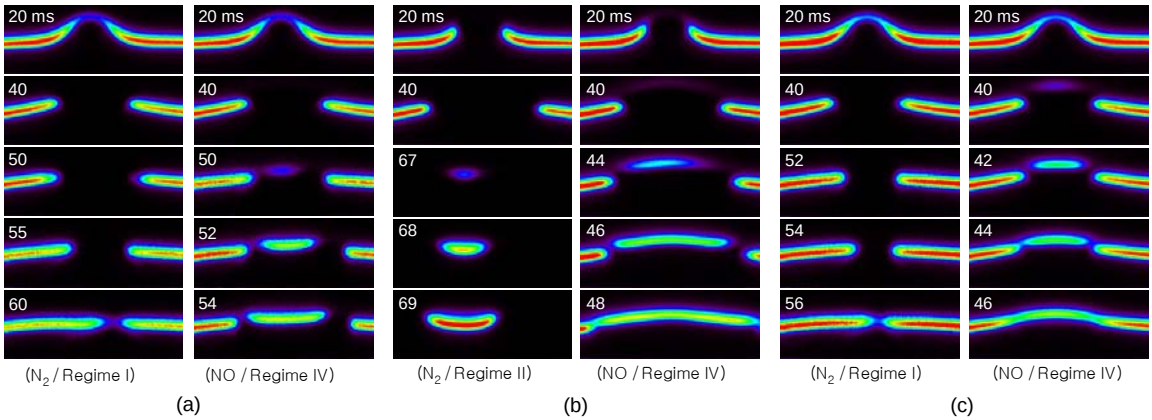


**Figure 5: Images of OH LIF during flame-vortex interaction with and without NO (a) $X_{H2}$ = 0.125, $T_{air}$ = 935 K (b) $X_{H2}$ = 0.11, $T_{air}$ = 951 K (c) $X_{H2}$ = 0.13, $T_{air}$ = 951 K**

Figures 6a and 6b show the effect of NO when the air temperature is 972 K and the recovery behavior corresponds to Regimes III and IV, respectively. The addition of NO decreases the induction time of re-ignition, but the change in the total recovery time is relatively modest compared to the cases in Fig. 5. In the recovery processes of Figs. 6a and 6b, though the addition of NO shifts the timing of the ignition, it does not change the recovery mechanism. The catalytic effect of NO decreases gradually as the air temperature increases, and it disappears completely if the air temperature is larger than 988 K. Fig. 6c shows the effect NO in the 'No extinction' case at the boundaries of Regimes I and IV in Fig. 4. The vortex-perturbed flame recovers soon by itself for both cases, and the addition of NO has no influence on the recovery process. This result implies that the catalytic effect of NO is significantly reduced when the flame is not fully extinguished.

Figure 7 shows the influence of NO on the recovery process as a function of fuel concentration and air temperature. A comparison of the re-ignition regimes with and without NO reveals several interesting features. First, the addition of NO increases the area of each regime and shifts

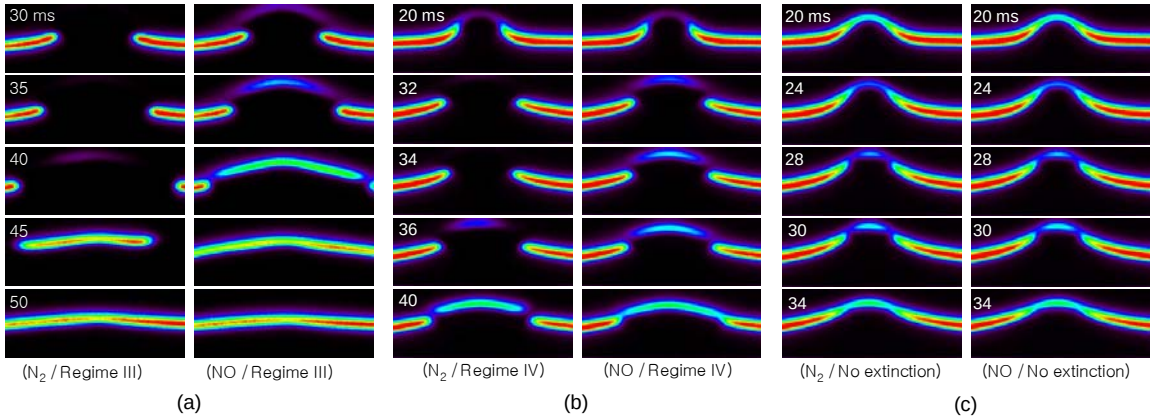


**Figure 6: Images of OH LIF during flame-vortex interaction with and without NO (a) $X_{H2}$ = 0.09, $T_{air}$ = 972 K (b) $X_{H2}$ = 0.11, $T_{air}$ = 972 K (c) $X_{H2}$ = 0.14, $T_{air}$ = 951 K**

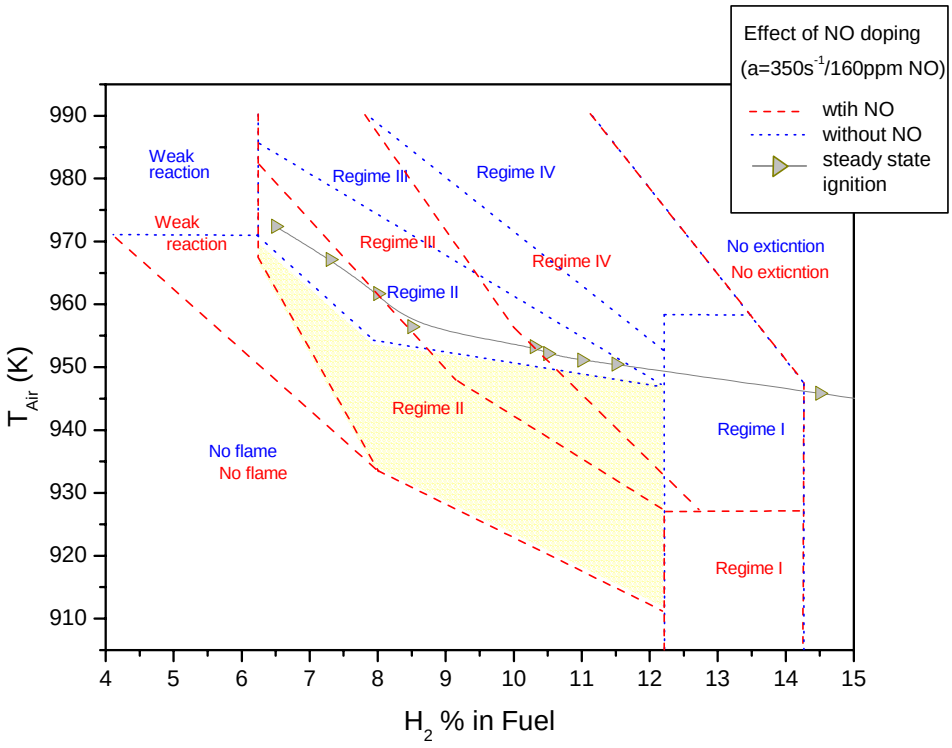


**Figure 7: Comparison of flame recovery process with and without NO doping**

the regimes toward lower temperatures and fuel concentrations. In this experiment, the NO starts to affect the system at $T_{air}$ = 910 K, and its catalytic effect disappears when the air temperature is larger than 988 K. As the air temperature approaches 988 K, the difference between the regime boundaries with and without NO disappears. The shaded area of Fig. 7 indicates the extended flammability limit with NO doping. A second important feature of the comparison in Fig. 7 is that boundary of the 'No extinction' region remains unchanged with the addition of NO. The initial extinction behavior for all of the conditions in Figs. 5 and 6 is also not effected by the NO doping. These results indicate that the NO has no influence on the susceptibility of the flame to extinction by the vortex. The third result is that NO has little effect on the edge-flame propagation. The Regime I boundary remains at $X_{H2}$ = 12.5 % when NO is added. The most significant change in Regime I is the shift of its upper boundary with Regime IV from $T_{air}$ = 955 K without NO to $T_{air}$ = 925 K with NO. However, in this part of Regime IV, the edge-flame propagation is very similar to Regime I until the ignition kernel and edge-flame merge. These results indicate that the catalytic effect of NO on the edge-flame propagation speed is not significant enough to overcome the increased radial outflow that the vortex produces. For the results presented here, NO is introduced only in the air flow. Additional experiments show that the results are identical when NO is introduced into both the fuel and air sides simultaneously. However, when the NO is only doped into the cold fuel mixture, the NO has no influence because of its relatively low diffusivity compared to $H_2$ and because the rates of the ignition reactions are most significant in the high-temperature fuel-lean conditions.

## 4. Direct numerical simulation

To understand the extinction and re-ignition process observed in the experiments and to investigate the NO effect on the process, we simulated the transient interaction of a flame with a vortex impulsively driven into the flame from the fuel stream. Two cases were considered with (Case 2) and without (Case 1) 160 ppm of NO included in the oxidizer stream as in the experiments. The oxidizer temperature and fuel concentration are chosen such that Cases 1 and 2 correspond to the experimental ignition Regimes I and IV, respectively.

Figure 8 shows the temporal evolution of $X_{OH}$ for the two cases in the flame/vortex interaction. However, unlike the experiments, the simulation results indicate that Case 1 resides in Regime II, and not in Regime I. Moreover, the location of re-ignition is not on the centerline as in the experiments, but is shifted radially off the centerline as shown in Fig. 8. This discrepancy may be due to the sensitivity of extinction/re-ignition to uncertainties associated with the radial mean velocity profiles at the boundaries and the selection of concentration and temperature parameters that are close to the boundary between Regimes I and II. Currently, plug flow is assumed such that there is no radial variation in the mean velocity at the boundaries, whereas, in the experiments, it is know that a velocity deficit exists near the polar axis due to the finite separation between the two nozzles [41]. As a result, the radial location of maximum scalar dissipation rate along the stoichiometric surface may differ between the experiments and computation. Efforts are currently underway to reconcile this difference.

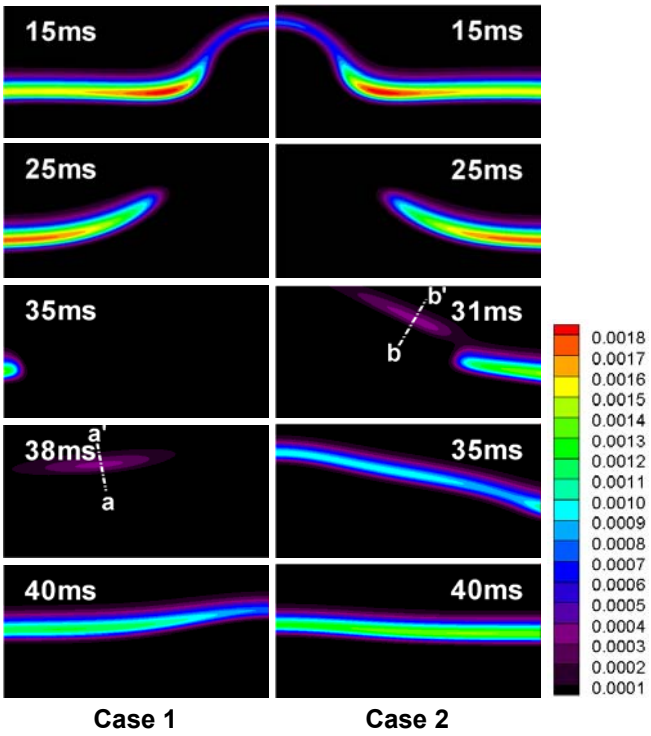


**Figure 8: Temporal evolution of $X_{OH}$ for cases 1 and 2.**

**Table 1: Selected elementary $H_2/O_2/NO_x$ reactions (Units are $cm^3$-mol-s-kcal-K, and $k = AT^n \exp(-E/RT)$ from Ref [32])**

| | | | *A* | *N* | *E* |
|---|---|---|---|---|---|
| R1 : | $H + O_2$ | = $O + OH$ | 3.547E+15 | -0.406 | 1.6599E+04 |
| R2 : | $H_2 + O$ | = $OH + H$ | 0.508E+05 | 2.670 | 0.6290E+04 |
| R3 : | $OH + H_2$ | = $H + H_2O$ | 0.216E+09 | 1.510 | 0.3430E+04 |
| R9 : | $O_2 + H + M$ | = $HO_2 + M$ | 1.475E+12 | 0.600 | 0.0000E+00 |
| R11: | $H + HO_2$ | = $OH + OH$ | 7.079E+13 | 0.000 | 2.9500E+02 |
| R12: | $O + HO_2$ | = $OH + O_2$ | 3.250E+13 | 0.000 | 0.0000E+00 |
| R13: | $OH + HO_2$ | = $O_2 + H_2O$ | 2.890E+13 | 0.000 | -4.9700E+02 |
| R27: | $H + NO_2$ | = $OH + NO$ | 1.320E+14 | 0.000 | 3.6200E+02 |
| R28: | $NO + HO_2$ | = $OH + NO_2$ | 2.110E+12 | 0.000 | -4.7900E+02 |

The simulations show that the region near the polar axis undergoes high scalar dissipation rate, $\chi$ (as high as 230 $s^{-1}$), or high tangential strain rate even after extinction occurs so that the outer region, which has lower scalar dissipation rate, is more favorable to re-ignition. In the presence of NO (Case 2) re-ignition occurs via mode IV where the outer annular edge-flame merges with the inner annulus ignition kernel. In the experiment where re-ignition occurs on the centerline the edge-flame annulus merges with an ignition disk. Note that re-ignition for Case 2 occurs sooner (31 ms) than for Case 1 (38 ms), attributed to the NO effect.

To understand the NO effect on extinction and re-ignition, we analyzed the elementary reactions involved in the process. For a $H_2/O_2/NO_x$ system, it is well known that a small amount of NO creates an alternate $HO_2$ consumption path such that the stable intermediate radical sink species, $HO_2$, can be converted to highly active radicals, OH, via $NO + HO_2 \Leftrightarrow OH + NO_2$ (R28). In addition to this reaction, $NO_2$ is used again to form OH and NO via $H + NO_2 \Leftrightarrow OH + NO$ (R27) and thus, NO enhances reaction by forming a catalytic cycle [16–18, 32, 42, 43]. Readers are referred to Table 1 for selected elementary reactions involved in the $H_2/O_2/NO_x$ chemistry.

The present simulation results also reveal the catalytic effect of NO on re-ignition. Figure 9 shows (a) the reaction rates of OH and temperature, and (b) the reaction rates of $HO_2$ and scalar

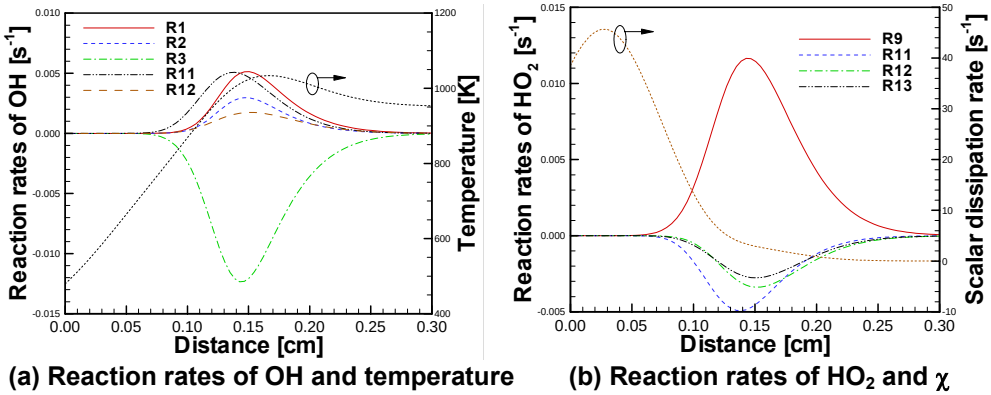


**(a) Reaction rates of OH and temperature** **(b) Reaction rates of $HO_2$ and $\chi$**

**Figure 9: Reaction rate budget, temperature and scalar dissipation rate along line a-a' for Case 1: (a) reaction rates of OH and temperature (b) reaction rates of $HO_2$ and scalar dissipation rate, $\chi$.**

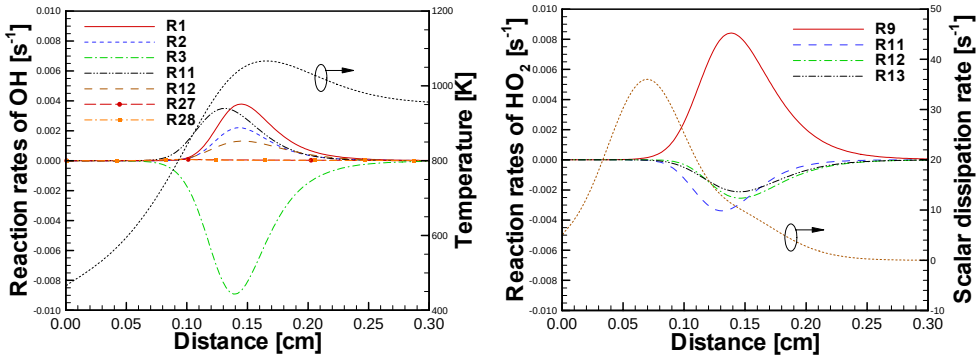


**Figure 10: Reaction rate budget, temperature and scalar dissipation rate along line b-b' for Case 2: (a) reaction rates of OH and temperature (b) reaction rates of $HO_2$ and scalar dissipation rate, $\chi$.**

dissipation rate along line a-a' at $t$ = 38 ms for Case 1. Figure 10 shows the same quantities along line b-b' at an earlier time, $t$ = 31 ms for Case 2. These two times correspond to ignition. It is apparent that near thermal runaway, the reactions occur within a similar temperature range for both cases but in the reaction region, the overall scalar dissipation rate for Case 2 is larger than that for Case 1. Therefore, the corresponding Damköhler numbers at the ignition kernel for both cases should be comparable since ignition occurs for both cases. In reality, the maximum Damköhler number, defined by the ratio of the reaction rate to diffusion of OH, is approximately 2.5 at the ignition kernel for both cases. The earlier ignition for Case 2 also implies that production of OH is enhanced by the catalytic effect of NO relative to Case 1.

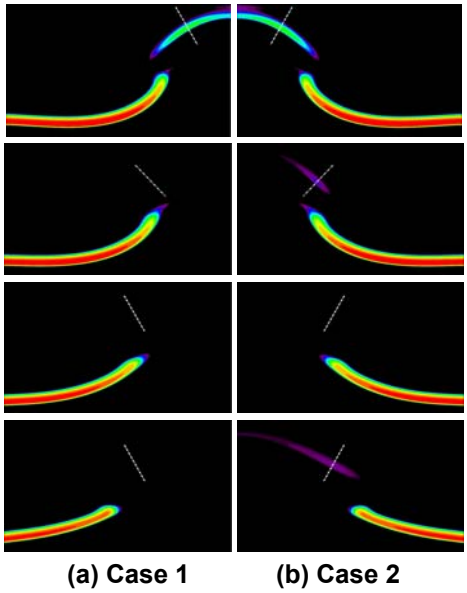


**Figure 11: Production rate of OH for Cases 1 and 2 and the location (white line) for budget analysis for reaction rate of OH. From top to bottom, t = 20, 22, 25, and 28 ms.**

However, since the generation of OH by $NO_x$ via R27 and R28 for Case 2 is negligible compared to the other reactions in Fig. 10, we examined the reaction rates of OH prior to thermal runaway. Figure 11 shows the production rate of OH at earlier times during the induction phase. Note that OH is formed towards the hot oxidizer stream in a concentrated region near the polar axis for Case 2 at 28 ms, prior to the rapid increase of $X_{OH}$ during ignition at 31ms, but such a concentrated OH region is not found for Case 1. To better understand the NO effect in this region 1-D cuts through the pre-ignition disk of OH were made (denoted by white line in Fig. 11) and a reaction flux analysis performed to determine the key elementary reactions responsible for OH production during the induction phase after the flame is extinguished and prior to thermal runaway.

The key elementary reactions of OH and the OH mole fraction are shown in Fig. 12 along the cuts denoted I n Fig. 11. For Case 1, the reactions responsible for OH production decrease by over 3 orders of magnitude after the flame is quenched. For Case 2, however, R27 and R28 sustain their reaction level through the entire re-ignition process even as other key reactions (R1, R2, R11 and R12) decrease after extinction until they start to rise again at 25 ms. The presence of the catalytic NO effect prevents the severity of the decline of these reactions. It also prevents OH concentration from dropping to levels two order of magnitude lower as in Case 1. Therefore, it is evident that the catalytic $NO_x$ cycle sustains the OH level following extinction such that re-ignition occurs sooner.

## 5. Concluding Remarks

The catalytic effect of NO on the extinction and re-ignition of a vortex-perturbed hydrogen flame is studied in a heated counter-flow configuration. The ignition behavior is measured for a wide range of temperatures and fuel concentrations with and without NO doping. When the air temperature is below the auto-ignition limit, the extinguished region of the flame recovers strictly by the edge-flame propagation. In contrast, if the air is heated above the auto-ignition temperature, an ignition kernel forms in the center of extinguished region, and the interaction between this ignition kernel and a propagating annular edge-flame produces additional recovery modes. The addition of 160 ppm of NO enhances re-ignition and significantly changes the flame recovery process. The additional NO enlarges the flammability limit and reduces the overall flame recovery time. The catalytic effect of NO facilitates the formation of a central ignition kernel but has minimal impact on the edge-flame propagation. Therefore, for mixture temperatures above the auto-ignition limit, the expansion of the central ignition kernel is the dominant recovery mechanism. The simulation results also confirm the catalytic effect of NO on ignition. The catalytic reactions of NO sustain OH levels and reduce $HO_2$ generation after flame extinction. These effects enable re-ignition to occur under conditions where re-ignition is not possible without NO doping. The present results show that accurate chemical mechanisms for NO reactions are important for accurate modeling of re-ignition processes and may be required for modeling of extinction and re-ignition in turbulent flames where these additional recovery modes may be active.

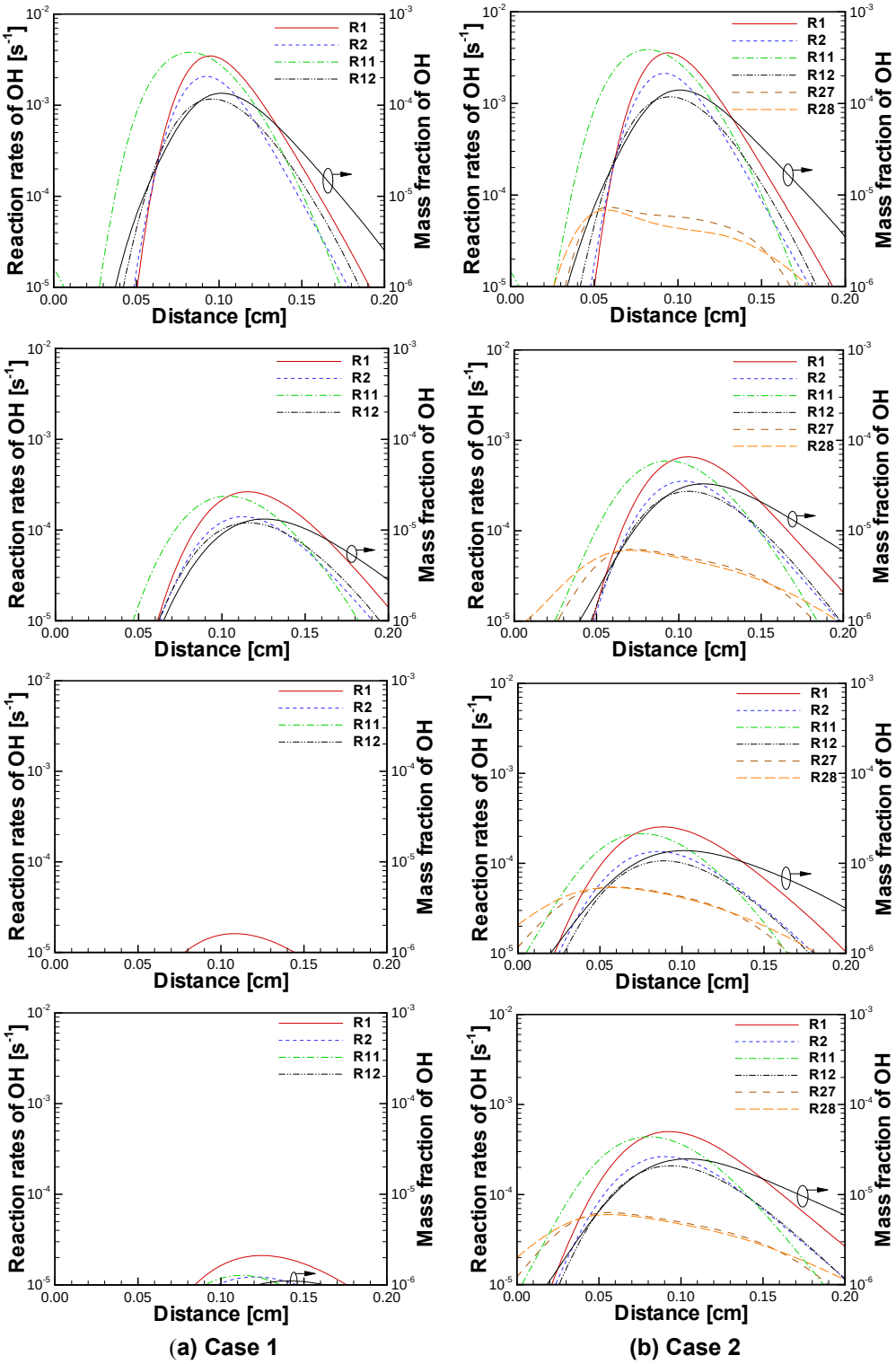


**Figure 12: OH reaction budget and OH mole fraction for cases 1 and 2. From top to bottom, t = 20, 22, 25, and 28 ms.**

## Acknowledgments

We thank Prof. F. L. Dryer of Princeton University for providing the $H_2/O_2/NO_x$ chemical mechanism and R. J. Sigurdsson of Sandia National Laboratories for assistance in the laboratory. This research was supported by the U.S. Department of Energy, Office of Basic Energy Sciences, Division of Chemical Sciences, Geosciences, and Biosciences. Sandia National Laboratories is a multiprogram laboratory operated by Sandia Corporation, a Lockheed Martin Company, for the U.S. Department of Energy under contract DE-AC04-94-AL85000. Uen Do Lee was supported by the Korea Research Foundation Grant funded by the Korean Government (MOEHRD) (KRF-2005-214-D00239).

## References

[1] C. Pantano, D. I. Pullin, *Combustion and Flame* 137 (2004) 295-305.
[2] R. R. Cao, S. B. Pope, *Combustion and Flame* 143 (2005) 450-470.
[3] G. L. Pellett, C. Bruno, W. chinitz, *38th AIAA/ASME/SAE/ASEE Joint Propulsion Conference & Exhibit* (2002) 1-38.
[4] B. Han, C. J. Sung, M. Nishioka, *Combustion Science and Technology* 176 (2004) 305-330.
[5] T. Faravelli, A. Franssoldati, E. Ranzi, *Combustion and Flame* 132 (2003) 188-207.
[6] G. Moreac, P. Dagaut, J. F. Roesler, M. Cathonnet, *Combustion and Flame* 145 (2006) 512-520.
[7] J. H. Bromly, F. J. Barnes, R. Madyczewsky, T. J. Edwards, B.S. Haynes, *Proceedings of the Combustion Institute* 24 (1992) 899-906.
[8] T. J. Held, C. V. Callahan, F. L. Dryer, *Chem. Phys. Process. Combust.* (1994) 270-273.
[9] P.H. Taylor, L. Cheng, B. Dellinger, *Combustion and Flame* 115 (1998) 561-567.
[10] P. Dagaut, F. Lecomte, S. Chevailler, M. Cathonnet, *Combustion Science and Technology* 148 (1999) 27-57.
[11] P. Dagaut, J. Luche, M. Cathonnet, *Combustion Science and Technology* 165 (2001) 61-84.
[12] P. Dagaut, A. Nicolle, *Combustion and Flame* 140 (2005) 161-171.
[13] P. F. Nelson, B. S. Haynes, *Proceedings of the Combustion Institute 25* (1994) 1003-1010.
[14] S. K. Prabhu, R. K. Bhat, D. L. Miller, N. P. Cernansky, *Combustion and Flame* 104 (1996) 377-390.
[15] W. R. Laster, P. E. Sojka, *Journal of Propulsion* 5 (1989) 385-390.
[16] P. Dagaut, F. Lecomte, J. Mieritz, P. Glarborg, *International Journal of Chemical Kinetics* 35 (2003) 564-575.
[17] G. Dayma, P. Dagaut, *Combustion Science and Technology* 178 (2006) 1999-2024.
[18] Y. Tan, C. G. Fotache, C. K. Law, *Combustion and Flame* 119 (1999) 346-355.
[19] P. Risberg, D. Johansson, J. Andrae, G. Kalghatgi, P. Björnbom, H. E. Ångström, *SAE Technical Paper Series* 2006-01-0416.
[20] S.Tanaka, F. Ayala, J. C. Keck, J. B. Heywood, *Combustion and Flame* 132 (2003) 219-239.
[21] V. S. Santoro, A. Gomez, *.Proceedings of the Combustion Institute* 29 (2002) 585-592.
[22] U. D. Lee, H. D. Shin, K. C. Oh, K. H. Lee, E. J. Lee, *Combustion and Flame* 144 (2006) 792-808.
[23] A. Lemaire, K. Zähringer, T.R. Meyer, J.C. Rolon, *Proceedings of the Combustion Institute 30* (2005) 475-483.
[24] R. Seiser, J.H. Frank, S. Liu, J.H. Chen, R.J. Sigurdsson, K. Seshadri, *Proceedings of the Combustion Institute* 30 (2005) 423-430.
[25] R. Seiser, K. Seshadri, E. Piskernik, A. Liñán, *Combustion and Flame* 122 (2000) 339-349.
[26] X.L. Zheng, J. Yuan, C.K. Law, *Proceedings of the Combustion Institute* 30 (2005) 415-421.
[27] G. Amantini, J. H. Frank, A. Gomez, *Proceedings of the Combustion Institute* 30 (2005) 313-321.
[28] G. Amantini, J. H. Frank, M. D. Smooke, A. Gomez, *Combustion and Flame,* 147 (2006) 133-149.
[29] G. Amantini, J. H. Frank, B. V. Bennett, M. D. Smooke, A. Gomez, 5th U.S. Combustion Meeting, San Diego, CA Paper #A04 (2007)
[30] V. S. Santoro, A. Liñán, A. Gomez, *Proceedings of the Combustion Institute* 28 (2000) 2039-2046.
[31] C. S. Yoo, H. G. Im, *Proceedings of the Combustion Institute* 30 (2005) 349-356.
[32] F. L. Dryer, *Private Communication*, 2006.
[33] C.G. Fotache, T. G. Kreutz, D. L. Zhu, C. K. Law, *Combustion Science and Technology* 109 (1995) 373-393.
[34] C. A. Kennedy, M. H. Carpenter, *Applied Numerical Mathematics* 14 (1994) 397–433.
[35] C. A. Kennedy, M. H. Carpenter, R. M. Lewis, *Applied Numerical Mathematics* 35 (2000) 177–264.

[36] R.J. Kee, F.M. Rupley, E. Meeks, J.A. Miller, *CHEMKIN-III: A Fortran Chemical Kinetics Package for the Analysis of Gas-Phase Chemical and Plasma Kinetics*, Sandia Rep. SAND96-8216, Sandia National Laboratories, 1996
[37] K. Seshadri, F. A. Williams, *International Journal of Heat and Mass Transfer* 21 (1978) 251–253.
[38] C. S. Yoo, Y. Wang, A. Troué, H. G. Im, *Combustion Theory and Modelling* 9 (2005) 617–646.
[39] C. S. Yoo, H. G. Im, *Combustion Theory and Modelling* 11 (2007) 259–286.
[40] S. James, C. K. Madnia, *Physics of Fluids* 8 (1996) 2400-2414.
[41] G. Amantini, J. H. Frank, M. D. Smooke, A. Gomez, *Combustion Theory and Modelling* 11 (2007) 47–42.
[42] M. A. Mueller, R. A. Yetter, F. L. Dryer, *International Journal of Chemical Kinetics* 31 (1999) 705–724.
[43] M. A. Mueller, R. A. Yetter, F. L. Dryer, *International Journal of Chemical Kinetics* 32 (2000) 317–339.